Available online at www.sciencedirect.com
ScienceDirect
Ceramics International 37 (2011) 2353–2358
CERAMICS INTERNATIONAL
www.elsevier.com/locate/ceramint

Doped ceria powders prepared by spray pyrolysis for gas sensing applications

Chin-Yi Chen *, Chin-Lung Liu

Department of Materials Science and Engineering, Feng Chia University, 100, Wenhwa Road, Seatwen, Taichung 40724, Taiwan

Received 22 November 2010; received in revised form 17 February 2011; accepted 20 March 2011
Available online 26 May 2011

Abstract

In the present study, ceria powder with and without gadolinium (Gd) or zirconium (Zr) dopants were synthesized by a spray pyrolysis (SP) process. The resulting powders (undoped CeO_2, Gd-doped ceria and Zr-doped ceria) were first mixed with organic binders, screen printed on alumina substrates, and then heat treated at 1200 °C for 2 h in air. Experimental results showed that the as-pyrolyzed powders were nanocrystalline and spherical in shape with uneven surfaces. After heat treatment, the powder coatings showed a 3-D network structure with interconnected pores exhibiting a high surface area. The electrical conductivity of CeO_2 was increased by the dope of Zr. The increasing rate of conductivity of ZDC (Zr-doped ceria) with decreasing oxygen pressure was also higher than that of undoped CeO_2. The CeO_2 and ZDC exhibited an *n*-type semiconductance in all the oxygen pressure regions, showing promise as candidates for sensor applications. The GDC (Gd-doped ceria) revealed a *p*-type and an *n*-type semiconductance in high- and low-oxygen pressure regions, respectively. The sensor applications of GDC are thus limited. Meanwhile, the ZDC exhibited a shorter response time due to its smaller grain size, showing a better oxygen sensing behavior.

Keywords: A. Powders: chemical preparation; B. Microstructure-final; B. Surfaces; C. Electrical conductivity; D. CeO_2; E. Sensors; Heat treatment

1. Introduction

To decrease exhaust gas emissions to meet the stringent requirements of environmental concerns and biodegradability, health, and safety regulations, controlling the air/fuel combustion ratio in industrial plants or in car emissions to enhance fuel efficiency is increasingly important [1,2]. The amount of oxygen in the exhaust gas indicates precisely the fuel conversion efficiency in a combustion system. An oxygen sensor plays a role in determining the oxygen content in the exhaust gas. The development of highly efficient oxygen sensors has thus been the aim of numerous researchers in recent years. Conventional solid-state electrolyte oxygen sensors are the most common type in the automotive industry. However, such potential-type sensors do not possess sufficient sensitivity due to their logarithmic response to the changes of oxygen concentration [3]. Moreover, a source of air is usually required as a reference for sensor operation. These characteristics may restrict the application of these types of sensors.

Resistive oxygen sensors have recently received great attention as candidates for research and development in this related field due to their relatively compact and simple structures and possibly lower costs [2]. Ceria, a pure non-stoichiometric *n*-type semiconductor (CeO_{2-x}) possessing a high oxygen-ion conductivity under an oxygen partial pressure of 10^5 Pa or lower, is capable of being an oxygen sensor material due to its good structural stability and high oxygen mobility [4]. Furthermore, oxygen vacancies can be introduced by substituting a fraction of the ceria with trivalent oxides [5,6], such as Y_2O_3 [7], Gd_2O_3 [8], and Sm_2O_3 [9] to increase the ionic conductivity of ceria.

In previous studies, many attempts have been made to prepare ceria for oxygen sensors including being hydrazine hydration [2], precipitation [10], mist pyrolysis techniques [11,12], and others [13,14]. However, to the best of our knowledge, a ceria powder with a hollow structure has not yet been reported for application in oxygen sensors. In the present study, hollow-structured ceria powders with and without Gd or Zr dopants were prepared by a spray pyrolysis/electrostatic

* Corresponding author. Tel.: +886 4 24517250x5313; fax: +886 4 24510014.
E-mail address: chencyi@fcu.edu.tw (C.-Y. Chen).

0272-8842/$36.00
doi:10.1016/j.ceramint.2011.05.079

deposition (SP/ESD) technique. The as-pyrolyzed powders were mixed with organics and screen-printed onto alumina substrates. The printed thick films were then heat treated to produce a porous structure for the evaluation of oxygen sensing properties. The phases of the pyrolyzed powders were identified by X-ray diffractometry (XRD). The microstructures of the resulting powders and thick films were observed by scanning electron microscopy (SEM).

2. Experimental procedures

Ceria powders with and without dopants were homogeneously prepared using a bench-scale spray pyrolysis/electrostatic deposition system. Details of the experimental set-up are described elsewhere [15,16]. To investigate the effect of Gd and Zr on the oxygen sensing properties of CeO_2, Gd and Zr were directly added into the CeO_2 ceramics during the preparation of precursor solutions. The precursor used for generation of CeO_2 powder in this study was cerium acetate (CeA). The chemical formula of CeA is $Ce(CH_3COO)_3{\cdot}1.5H_2O$ (99.9%, Alfa Aesar, A Johnson Matthey Co.), and the chemical is a reagent grade of >99% purity. The precursors of the dopants were gadolinium acetate tetrahydrate (GdA, from Strem Chemicals Inc., Newburyport, MA) and zirconium hydroxyl acetate (ZrA, from Aldrich Chemical Inc., Milwaukee, WI). Both salts were also reagent grade (>99% purity). The chemical formulas of GdA and ZrA are $Gd(CH_3COO)_3{\cdot}4H_2O$ and $Zr(OH)_x(CH_3COO)_{4-x}$, where $x = 2.64$. The molecular weights of CeA, GdA, and ZrA reported by the manufacturers are 344, 406.45, and 216, respectively. The precursor solutions were prepared as the CeA containing GdA or ZrA in a molar ratio of 10/90 for Gd_2O_3/CeO_2 (GDC) or ZrO_2/CeO_2 (ZDC). The concentration of precursor solutions (CeA + GdA) or (CeA + ZrA) in de-ionized water, was prepared as 1.0 wt.% for atomization.

The as-pyrolyzed powders were mixed with terpineol (J.T. Baker Co., USA) and ethyl cellulose (48%, Aldrich Co., USA) to result in pastes, and then coated onto Al_2O_3 substrates (20 mm × 20 mm × 0.64 mm) by screen printing. The weight ratios of the terpineol to ethyl cellulose and the organics to powder were set at 94:6 and 80:20, respectively. To remove the organics and confirm the formation of the oxides for the powder coatings, the screen-printed thick films were calcined at a temperature of 500 °C for 5 h in air (TF55035A, Lindberg/Blue M, USA). The heating and cooling rates were 5 °C/min. Subsequently, the films were heat treated at 1200 °C for 2 h in air (BF51314C, Lindberg/Blue M, USA). The heating and cooling rates were both 5 °C/min.

The morphology of as-pyrolyzed powders and heat-treated powder coatings was observed using field emission scanning electronic microscopy (FE-SEM, JSM-6700F, JEOL, Japan). The phases were identified using X-ray diffractometry (XRD, D8 SSS, Bruker, German). The heat treated thick films were then screen-painted with a platinum (Pt) paste at both ends for measurement of sensing property, as shown in Fig. 1. Two flat-pressed Pt wires with a diameter of 0.5 mm (thermocouple grade) were attached onto the Pt paste. The as-pasted

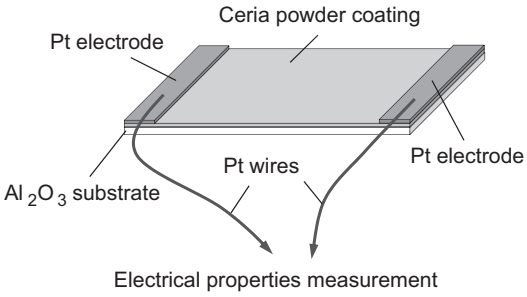

Fig. 1. Schematic drawing of the measurement of SP powder coating for sensing properties.

specimens, connected with two Pt wires, were heated to 1000 °C for 20 min in air to cure the Pt electrode. The electrical conductivities of the films were recorded in a tubular furnace at a temperature range from 750 °C to 850 °C under various oxygen partial pressures by a data acquisition apparatus (Agilent 34970A, USA). An accurately calibrated homemade oxygen sensor (mixed potential-type zirconia-based) was placed in the downstream of the tubular reactor for the measurement of oxygen partial pressure. The oxygen sensor response time of the coated films was determined by recording their corresponding resistivities with a sudden change of oxygen partial pressure [12,17]. The oxygen partial pressure was suddenly changed from 1.0 atm to 0.01 atm. The sensor output and oxygen partial pressure were measured as a function of time.

3. Results and discussion

Fig. 2 shows the XRD patterns of the as-pyrolyzed undoped CeO_2, GDC, and ZDC powders. Note that the resulting powders were identified as a CeO_2 phase with poor crystallinity. The broadened peaks indicate that these powders were nanocrystalline, with a crystallite size ranging from ca. 4.5 nm to 8 nm. After doping with Gd and Zr, no significant peak shift appeared in the XRD patterns. However, with the more significant peak

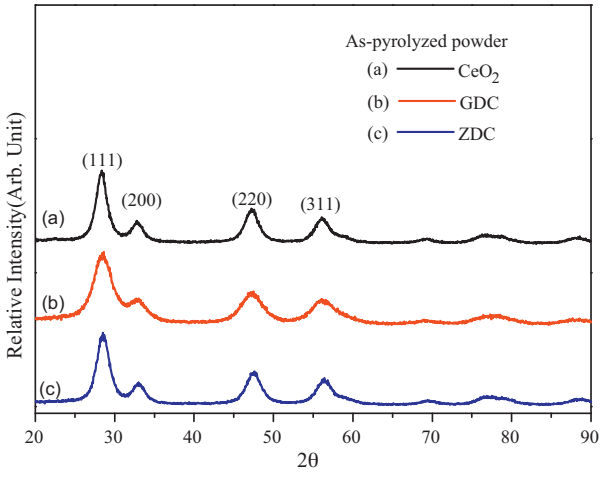

Fig. 2. XRD patterns of as-pyrolyzed (a) CeO_2, (b) GDC, and (c) ZDC powders.

broadening, the crystallite size of CeO_2 tended to decrease. The mean grain sizes of CeO_2, GDC and ZDC powders calculated by Scherrer's formula are 7.0, 3.7 and 5.3 nm, respectively, values that have been confirmed by HR-TEM microscopy in our previous study [18]. Though not shown here, the presence of Gd and Zr in CeO_2 can be determined by energy-dispersive X-ray spectroscopy (EDX). Fig. 3 shows the SEM micrographs of the as-pyrolyzed CeO_2, GDC and ZDC powders. Note that the particles were spherical in shape, with some cavities. The particle sizes of these powders exhibited broad size distributions ranging from ca. 100 nm to several microns. The insets show their corresponding TEM images of the particles, which exhibit hollow structures due to the surface precipitation of the CeA precursors during SP [18,19]. Some fractured particles are observed, their inner surfaces have been revealed because they were not able to endure the shrinkage deformation that occurred during cooling in SP [20]. The doping with Gd and Zr did not have an obvious influence on the microstructure of the pyrolyzed CeO_2 powder.

These powders were then mixed with some organics and screen-printed onto the Al_2O_3 substrates. The morphologies of the coatings are shown in Fig. 4, which shows the coatings after heat treatment at 1200 °C. As can be seen, the coatings have a porous structure with grown grains, exhibiting a high surface area. Such a porous structure tends to enhance gas reaction on the surface of the material, though the sensor is simply responding to the change in bulk point defect controlled by the change in oxygen partial pressure. A porous thick-film based sensor is thus preferred for the gas to gain access to the active sites on ceria surfaces. Moreover, the mean grain sizes of CeO_2, GDC, and ZDC thick films are 420, 130 and 260 nm, respectively. The grain growth of the CeO_2 coating is significantly inhibited by doping with Gd and Zr during heat treatment. In addition, after heat treatment, not only can the pores between the sites of original particles be observed, but also the inner surfaces in the hollow particles can be revealed. The side-view images of the coatings shown in their corresponding insets reveal a particulate 3-D network structure with interconnected pores.

Fig. 5 shows the electrical conductivities of CeO_2 thick film as a function of oxygen partial pressure at various temperatures. Notice that the conductivity of the undoped CeO_2 coating increases with a decrease in oxygen partial pressure, exhibiting an *n*-type semiconductance in the region of oxygen partial pressure from 1 atm to 10^{-20} atm. This can be attributed to the increase in Ce^{3+} when reduction of CeO_2 occurs in the lean oxygen partial pressure. Moreover, the conductive behavior of the CeO_2 coating was revealed to be almost the same at different temperatures. The conductivity of the CeO_2 coating was enhanced when temperature was elevated.

Fig. 6 shows the electrical conductivities of GDC thick film as a function of oxygen partial pressure and temperature. A slight tendency of *p*-type semiconductance of the GDC coating can be noticed in the region of high oxygen partial pressure. In the case of CeO_2, oxygen vacancy concentration may be increased by doping with Gd^{3+} ions to substitute for the sites of Ce^{4+} ions. This may result in the ionic conductance of the GDC coating in high-oxygen pressure regions. When the oxygen partial pressure was decreased to the region of 0.21–10^{-10} atm, the conductivity showed no significant change due to the transition between the electronic and ionic conductances. GDC is thus not suitable for

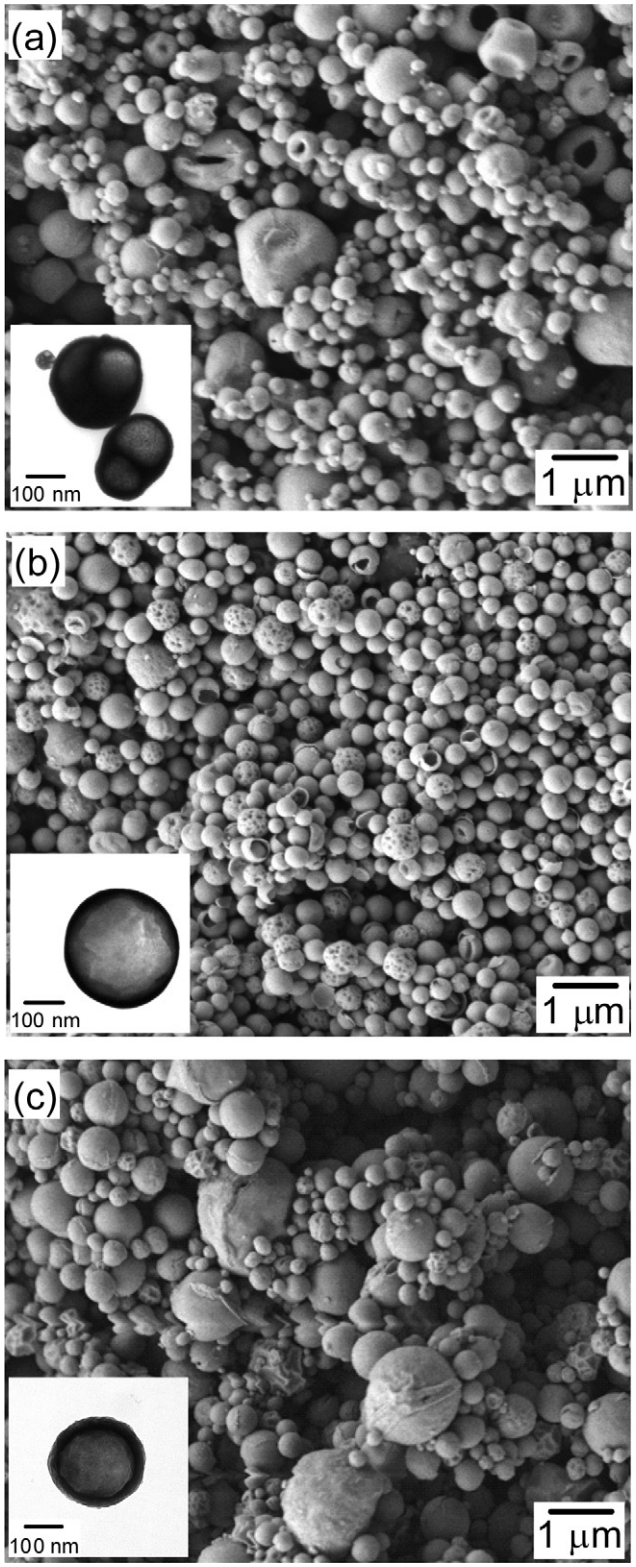

Fig. 3. SEM micrographs of the as-pyrolyzed (a) CeO_2, (b) GDC, and (c) ZDC powders. The insets show the corresponding TEM images of the single particles.

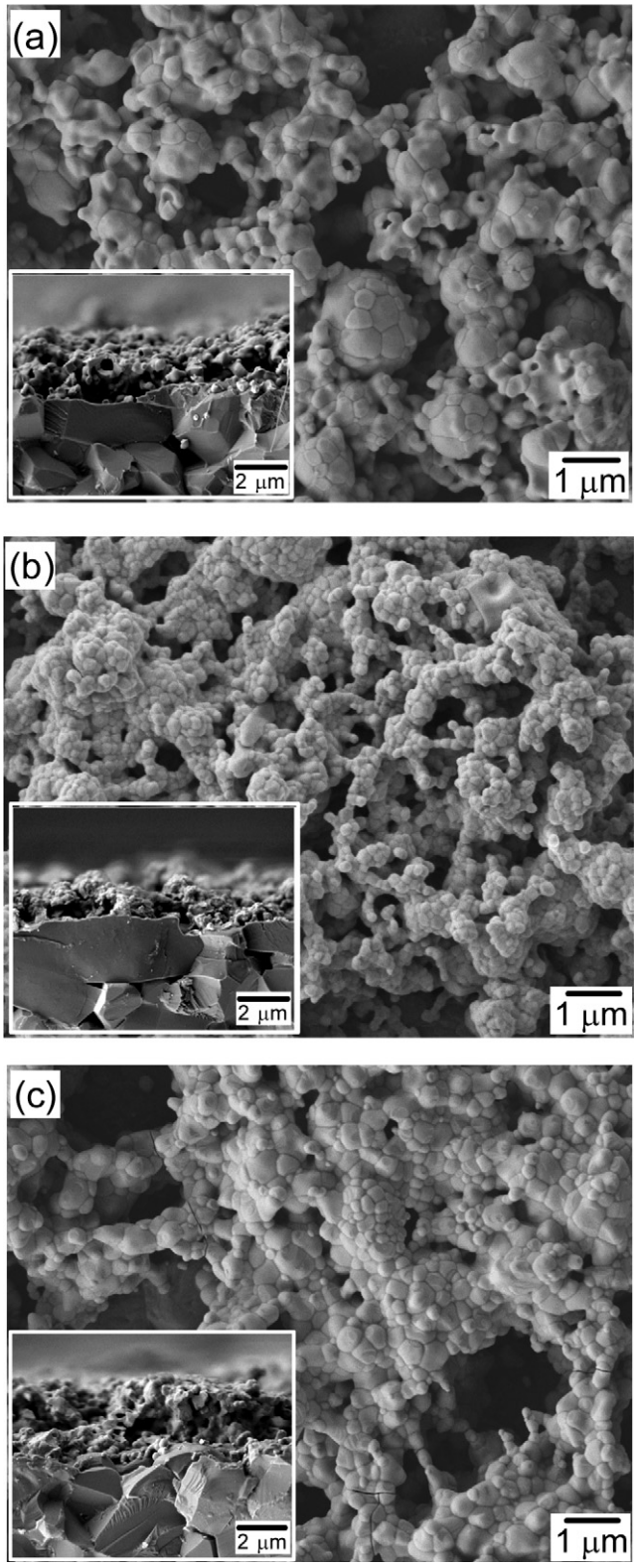

Fig. 4. Top-view SEM micrographs of (a) CeO_2, (b) GDC and (c) ZDC powder coatings. The insets show their corresponding side-view images.

use in resistive oxygen sensors in such oxygen pressure regions. As the oxygen partial pressure further decreased to the lean region, the conductivity increased to exhibit an *n*-type semiconductance due to the majority electronic conductance.

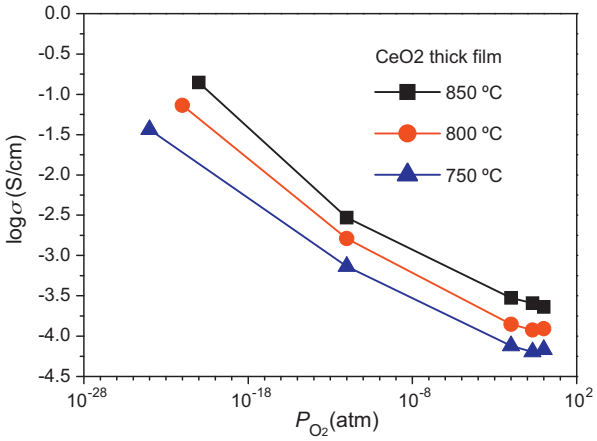

Fig. 5. Electrical conductivity of CeO_2 thick film at various temperatures as a function of oxygen partial pressure.

To investigate effects of the dopant with different valences on the sensing properties of CeO_2, Zr^{4+} was doped into CeO_2 for comparison to the GDC. Fig. 7 shows the electrical conductivities of ZDC thick film as a function of oxygen partial pressure and temperature. Note that the ZDC exhibited a relatively high conductivity compared to those in Figs. 5 and 6, showing an obvious *n*-type semiconductive behavior from the high-oxygen pressure region to the low one. This trend is similar to that observed in undoped CeO_2 (Fig. 5). Because Zr and Ce possess the same valence states (+4), an oxygen vacancy concentration in CeO_2 will not be further generated when Ce^{4+} is substituted with Zr^{4+}. The lattice shrinkage of CeO_2 due to doping with Zr^{4+} may shorten the distance of the electron hopping conduction [10]. Thus, the electrical conductivity of the ZDC coating was enhanced.

The conductivity of semiconductor ceramics, σ_e, can be expressed in terms of the oxygen partial pressure, P_{O_2}, as:

$$\sigma_e = A(T)P_{O_2}^{-1/n}$$

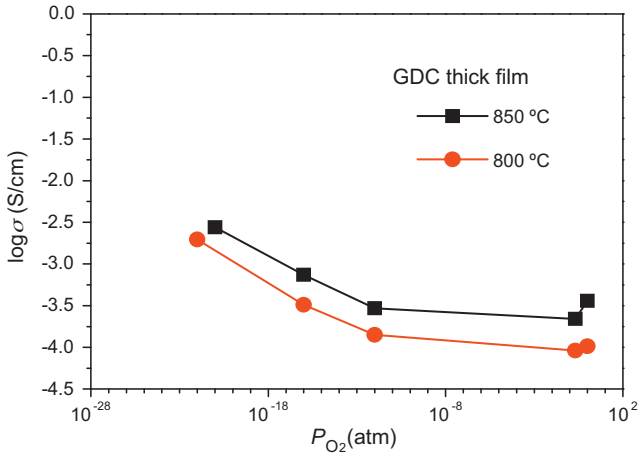

Fig. 6. Electrical conductivity of GDC thick film at various temperatures as a function of oxygen partial pressure.

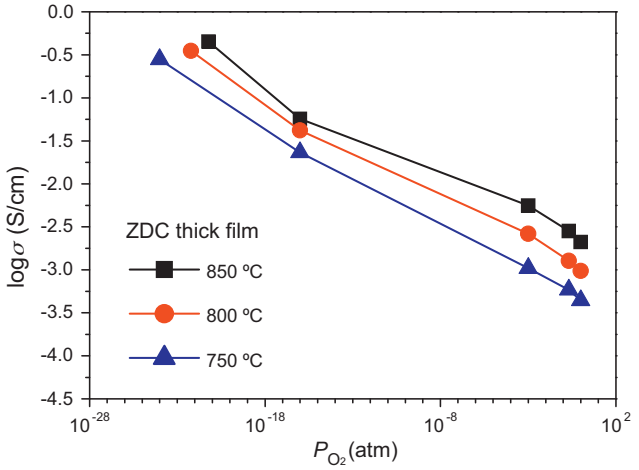

Fig. 7. Electrical conductivity of ZDC thick film at various temperatures as a function of oxygen partial pressure.

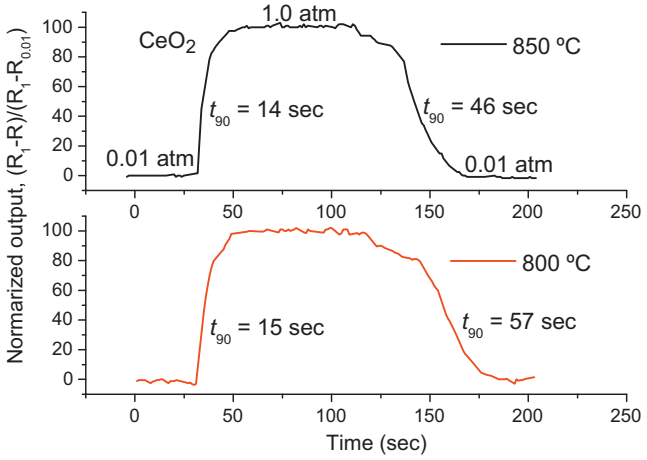

Fig. 8. Dynamic response of the CeO_2 thick film sensitivity to change in oxygen pressure at 800 °C and 850 °C.

where $A(T)$ is the temperature dependent constant. Theoretically, the value of n can be, respectively calculated as 4 for extrinsic conductance and 6 for intrinsic conductance from the defect chemistry of semiconductive ceramics [3]. In Figs. 5–7, the conductivity of the thick films increases with elevated operation temperature. According to the slope calculation, however, the values of n for the thick films range from 7.8 to 10.1 at various operation temperatures, as shown in Table 1. This may result from many variables, such as grain size, porosity, lattice strain, and different amounts of Ce^{3+} in CeO_2. Further investigation is still in progress. Unlike that of ZDC, the conductance of ceria may be converted from n-type semiconductance into ionic conductance due to the increase of oxygen ion vacancies by adding Gd^{3+} to ceria (GDC). Such an addition may increase the n value in ceria-based ceramics. Moreover, the value of n for reduced CeO_2-based ceramics has been reported to vary with the increase of Ce^{3+} at a temperature range of 750−850 °C in lean oxygen partial pressure [6,21]. As can be seen in Table 1, the ZDC exhibited a higher value of n than the undoped CeO_2 due to the enhancement of conductivity of ZDC in the oxygen partial pressure region from 0.01 to 1.0 atm (Fig. 7), suggesting that the amount of Ce^{3+} may be increased by doping CeO_2 with Zr. This also agrees well with the results reported in the literature [6,22].

Figs. 8 and 9 show, respectively the dynamic responses for the CeO_2 and ZDC coating sensitivities to oxygen gas changes at temperatures of 800 and 850 °C. Response time (t_{90}) is defined as the time when the ratio $(R_{1.0} - R)/(R_{1.0} - R_{0.01})$ becomes 0.9 after the oxygen partial pressure changes suddenly, where $R_{1.0}$ and $R_{0.01}$ are the stable electrical resistivities in oxygen partial pressures of 1.0 and 0.01 atm, respectively [11]. Notice that a relatively short t_{90} of about 14 s for CeO_2 and ZDC thick films was obtained when the oxygen partial pressure suddenly increased from 0.01 atm to 1.0 atm. No such obvious difference in t_{90} was found when the oxygen partial pressure changed from low to high. Also, the operation temperature did not seem to influence the response time when oxygen partial pressure was suddenly increased, whereas a prolonged t_{90} for both coatings was obtained after a sudden decrease of oxygen partial pressure. However, the temperature still did not show any influence on the t_{90} for ZDC thick film. The ZDC coating exhibited a shorter response time than the undoped CeO_2 coating when the oxygen partial pressure suddenly decreased. This may be attributed to the smaller grain size of ZDC thick film, which revealed better sensor kinetics, whether they are controlled by the mechanisms of oxygen vacancy diffusion or surface reaction [23,24].

Table 1
The value of n in $\sigma_e \propto P_{O_2}^{-1/n}$ of the CeO_2, GDC and ZDC thick films at various temperatures.

Temperature (°C)	CeO_2	GDC	ZDC
	n in $\sigma_e \propto P_{O_2}^{-1/n}$		
850	7.8	9.3	10.1
800	8.0	8.6	9.3
750	8.7	–	9.0

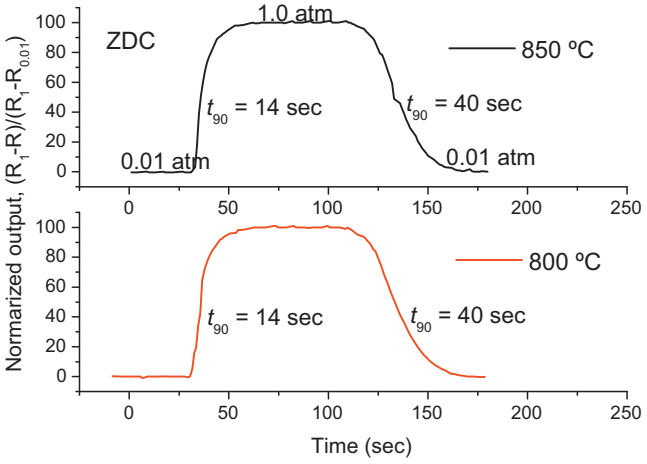

Fig. 9. Dynamic response of the ZDC thick film sensitivity to change in oxygen pressure at 800 °C and 850 °C.

4. Conclusions

Spray pyrolyzed undoped CeO_2, GDC and ZDC powders were coated onto Al_2O_3 substrates for the evaluation of oxygen sensing properties in the present study. The crystallite size of as-pyrolyzed CeO_2 can be decreased by the addition of Gd and Zr. Even after heat treatment at 1200 °C, the doped CeO_2 thick films still exhibited smaller grain sizes. Undoped CeO_2 and ZDC can be considered as promising candidates for oxygen sensor applications due to their *n*-type semiconductance in all regions of oxygen partial pressure. The increased amount of Ce^{3+} in CeO_2 resulted from doping with Zr, which may cause enhancement in conductivity when operation temperature is elevated. Furthermore, the ZDC thick film exhibited a faster dynamic response to the change in oxygen partial pressure, revealing better sensing properties than the undoped CeO_2. The GDC thick film exhibited, respectively a *p*-type and an *n*-type semiconductance in the high- and low-oxygen pressure regions, resulting in restricted applications of the oxygen sensors.

Acknowledgements

The authors would like to thank the National Science Council of Taiwan for financially supporting this work under Grant No. NSC 99-2628-E-035-002. The authors also thank the FCU for partially financial support.

References

[1] A.D. Brailsford, E.M. Logothetis, Selected aspects of gas sensing, Sens. Actuators B 52 (1998) 195–203.
[2] S.V. Manorama, N. Izu, W. Shin, I. Matsubara, N. Murayama, On the platinum sensitization of nanosized cerium dioxide oxygen sensors, Sens. Actuators B 89 (2003) 299–304.
[3] P. Jasinski, T. Suzuki, H.U. Anderson, Nanocrystalline undoped ceria oxygen sensor, Sens. Actuators B 95 (2003) 73–77.
[4] J.W. Dawicke, R.N. Blumenthal, Oxygen association pressure measurements on nonstoichiometric cerium dioxide, J. Electrochem. Soc. 133 (1986) 904–909.
[5] J. Van herle, T. Horita, T. Kawada, N. Sakai, H. Yokokawa, M. Dokiya, Low temperature fabrication of (Y,Gd,Sm)-doped ceria electrolyte, Solid State Ionics 86–88 (1996) 1255–1258.
[6] M. Mogensen, N.M. Sammes, G.A. Tompsett, Physical, chemical and electrochemical properties of pure and doped ceria, Solid State Ionics 129 (2000) 63–94.
[7] Y. Xiong, K. Yamaji, T. Horita, N. Sakai, H. Yokokawa, Electronic conductivity of 20 mol% $YO_{1.5}$ doped CeO_2, J. Electrochem. Soc. 149 (2002) E450–E454.
[8] J.M. Im, H.J. You, Y.S. Yoon, D.W. Shin, Synthesis of nano-crystalline $Gd_{0.1}Ce_{0.9}O_{2-x}$ for IT-SOFC by aerosol flame deposition, Ceram. Int. 34 (2008) 877–881.
[9] M. Chen, B.H. Kim, Q. Xu, B.K. Ahn, W.J. Kang, D.P. Huang, Study on the relationship between the defect and dielectric properties of ZnO-doped $BiNbO_4$ ceramic, Ceram. Int. 35 (2009) 1335–1339.
[10] N. Izu, N. Oh-hori, M. Itou, W. Shin, I. Matsubara, N. Murayama, Resistive oxygen gas sensors based on $Ce_{1-x}Zr_xO_2$ nano powder prepared using new precipitation method, Sens. Actuators B 108 (2005) 238–243.
[11] N. Izu, W. Shin, N. Murayama, S. Kanzaki, Resistive oxygen gas sensors based on CeO_2 fine powder prepared using mist pyrolysis, Sens. Actuators B 87 (2002) 95–98.
[12] N. Izu, W. Shin, I. Matsubara, N. Murayama, Kinetic behavior of resistive oxygen sensor using cerium oxide, Sens. Actuators B 100 (2004) 411–416.
[13] H.J. Park, G.M. Choi, Oxygen permeability of gadolinium-doped ceria at high temperature, J. Eur. Ceram. Soc. 24 (2004) 1313–1317.
[14] B. Elyassi, N. Rajabbeigi, A. Khodadadi, S.S. Mohajerzadeh, M. Sahimi, An yttria-doped ceria-based oxygen sensor with solid-state reference, Sens. Actuators B 103 (2004) 178–183.
[15] C.Y. Chen, C.K. Lin, Y.R. Lyu, H.H. Lin, W.H. Tuan, Pseudocapacitive manganese oxide prepared by a spray pyrolysis/electrostatic deposition technique, Adv. Sci. Technol. 45 (2006) 1896–1901.
[16] C.-Y. Chen, Y.-R. Lyu, C.-Y. Su, H.-M. Lin, C.-K. Lin, Characterization of spray pyrolyzed manganese oxide powders deposited by electrophoretic deposition technique, Surf. Coat. Technol. 202 (2007) 1277–1281.
[17] J. Gerblinger, U. Lampe, H. Meixner, Sensitivity mechanism of metal oxides to oxygen detected by means of kinetic studies at high temperatures, Sens. Actuators B 25 (1995) 639–642.
[18] S.-J. Shih, Y. Huang, Y.-R. Lyu, C.-Y. Chen, Cross-sectional observation of yttrium and nickel oxide doped ceria powder, J. Nanosci. Nanotechnol. 9 (2009) 3898–3903.
[19] S.-J. Shih, L.-Y.S. Chang, C.-Y. Chen, K.B. Borisenko, D.J.H. Cockayne, Nanoscale yttrium distribution in yttrium-doped ceria powder, J. Nanopart. Res. 11 (2009) 2145–2152.
[20] S.-J. Shih, K.B. Borisenko, L.-J. Liu, C.-Y. Chen, Multiporous ceria nanoparticles prepared by spray pyrolysis, J. Nanopart. Res. 12 (2010) 1553–1559.
[21] O. Toft Sørensen, Thermodynamic studies of the phase relationships of nonstoichiometric cerium oxides at higher temperatures, J. Solid State Chem. 18 (1976) 217–233.
[22] F. Zhang, C.-H. Chen, J.M. Raitano, J.C. Hanson, W.A. Caliebe, S. Khalid, S.-W. Chan, Phase stability in ceria-zirconia binary oxide nanoparticles: the effect of the Ce^{3+} concentration and the redox environment, J. Appl. Phys. 99 (2006) 084313–084320.
[23] R.K. Sharma, M.C. Bhatnagr, Improvement of the oxygen gas sensitivity in doped TiO_2 thick films, Sens. Actuators B 56 (1999) 215–219.
[24] U. Schönauer, Response times of resistive thick-film oxygen sensors, Sens. Actuators B 4 (1991) 431–436.